Indonesian Journal of Electrical Engineering and Computer Science
Vol. 42, No. 2, May 2026, pp. 318~336
ISSN: 2502-4752, DOI: 10.11591/ijeecs.v42.i2.pp318-336

Parametric analysis and mitigation of Ferroresonance in ungrounded power transformers: Algeria power plant approach

Mohammed Boukaf[1], Saliha Boutora[2], Hamid Bentarzi[2]
[1]Department of Electrical Engineering, Faculty of Electrical Engineering and Computer Science, University Mouloud Mammeri, Tizi Ouzou, Algeria
[2]Laboratory Signals and Systems, Institute of Electrical and Electronic Engineering, University M'hamed Bougara, Boumerdes, Algeria

Article Info

Article history:

Received Jul 28, 2025
Revised Mar 18, 2026
Accepted Mar 26, 2026

Keywords:

Ferroresonance
Grading capacitance
MATLAB/Simulink
Shunt capacitance
Ungrounded power transformer
Zigzag transformer

ABSTRACT

Ferroresonance in ungrounded power transformers is extremely dangerous for electric systems, causing serious overvoltage, equipment damage, and system instability. Until now, there have been fewer quantitative, parametric analytical studies and verified mitigation methods for real power systems. Although there has been a qualitative study of Ferroresonance, few have provided rigorous parametric assessments and validated mitigation actions for modern power plants at utility scale. This work fills these gaps through in-depth parametric analysis of the so-measured and so-calculated values and a validation of zigzag transformer grounding for the Ras Djinet 1131 MW power plant, serving as a case study in Algeria. This paper establishes a nonlinear mathematical model that reflects transformer saturation characteristics, grading capacitance (Cg), shunt capacitance (Csh), and magnetization resistance (Rm), and implements it in MATLAB/Simulink. Fundamental and chaotic Ferroresonance modes are identified using parametric sweeps spectral analysis (FFT). Act two: Modeling and validating zigzag grounding transformer mitigation. The study finds Cg (0.5–7 µF) increases strengthen Ferroresonance overvoltage, while Csh (0.3_7µF) and Rm (1500–65860Ω) reduce it, offering a damping effect, reducing peak voltages. Spectral analysis reveals the fundamental mode (dominated by 50 Hz), the Quasi-Periodic Mode, and the chaotic mode (multiple frequency components). With a zero-sequence current path, a zigzag grounding implementation completely removes Ferroresonance in all tested cases.

Corresponding Author:

Saliha Boutora
Laboratory Signals and Systems, Institute of Electrical and Electronic Engineering
University M'hamed Bougara of Boumerdes
Boulevard de l'indépendance, 35000 Boumerdes, Algeria
Email: s.boutora@univ-boumerdes.dz

1. INTRODUCTION

Ferroresonance is a complex nonlinear phenomenon in power systems that arises when the saturable inductance of a transformer forms a series resonance circuit with the network capacitances, typically due to cable capacitances. Cable grading capacitors, or stray capacitances [1]. This phenomenon is particularly common in ungrounded or isolated neutral systems, where single-phase switching actions can energize the transformer windings via capacitive coupling [2]. The nonlinear magnetization characteristic of transformer cores supports stable sustained oscillations at fundamental, sub-harmonic, or quasi-periodic frequencies, with severe overvoltages (2-5 pu), overcurrents, and indeed even catastrophic equipment damage [3], [4]. But in a power network that does not connect the neutral wire to ground (not specifically referring to this, but rather

home circuits), ferroresonance can occur during switching transitions. This condition often occurs when capacitor banks are switched out or when sequences are run to clear faults [5].

The modelling of ferroresonance has moved from simple analytical rough methods to the more sophisticated electromagnetic transient simulations (EMT). The basic representation of a series LC circuit with nonlinear magnetisation curves, modelled after transformer test data [6]. Recently, for classifying ferroresonance regimes. Time-domain simulations are extensively performed on platforms such as MATLAB/Simulink and ATP- EMTP [7], [8]. But most studies are conducted on simplified networks or common transformer models and do not use practical cases with measured parameters. A crucial shortcoming lies in models that have been validated with actual power plant data and provide thorough parameter verification.

The effects of system parameters on ferroresonance properties have been studied by several scholars. The studies reported by [9], [10] showed that grading capacitance (Cg) plays a major role in VT ferroresonance, where higher values of Cg contribute to the continuation of oscillations. The effects of shunt capacitance (Csh) were studied, which indicated damping in some regions. The magnetization resistance (Rm), which is equivalent to core losses, was investigated with [11], [12].

Ferroresonance appears in different modes of operation: basic (periodic at system frequency), subharmonic (periodic at a fraction of the system frequency), quasi-periodic (multi-frequency–incommensurate), and chaotic (aperiodic) [13]. Detection methods comprise FFT spectral analysis [14]. However, despite these achievements, time-domain-based model classification remains challenging in practical cases due to the lack of systematic analysis of frequency- or nonlinear dynamical characteristics [15]. It is a limitation in the understanding of mode transitions and parameter sensitivity.

Many mitigation methods have been proposed and tested. Passive methods are the use of (1) resistive damping in series or parallel with transformer windings [16] effective, but they cause continuous losses; (2) neutral grounding via resistors or reactors [17] provide zero-sequence paths and (3) zigzag grounding transformers [18], [19] artificial neutrals in delta-connected systems. Active methods use solid-state ferroresonance suppression circuits (SSFSC) [20] and protection relays with commutated loads [21], which can efficiently detect and suppress the same. Although the principle of zigzag grounding appears to be beneficial in theory, there are few design details, validation of simulation models, or comparisons of effectiveness under large-power transformer operating conditions in real power plant arrangements. Few mitigation analyses have evolved into practical applications.

From the literature review, four critical gaps are found: (1) little work employs complete real power plant data with measured transformer characteristics and system parameters; (2) statistical correlation technique and reasonable parameter selection method (like Rudenberg's one etc.,), are still limited or do not exist at all; (3) joint spectral, and nonlinear analysis is rarely used in case studies; and (4) lossy design specifications for large power transformers are also insufficient. These deficiencies limit the direct application of ferroresonance studies to practical absolute protection and system design.

The need for the new study is to fill these gaps, and this will be achieved by conducting a comprehensive investigation of ferroresonance in the ungrounded transformers at Ras Djinet 1131 MW. The specific aims and contributions are:

Develop and test a nonlinear ferroresonance model that includes measured transformer magnetisation, standing capacitances obtained from graphical methods, and guaranteed distribution system parameters from Djinet plant data sheets. Use mathematical parameter scanning of Cg: 0.5-7 µF, Csh: 0.3-7 µF, and Rm: 1500-65860 Ω) with statistical correlation analysis to quantify parameter effects. Use the FFT spectral analysis and frequency domain characterisation to distinguish quantitatively between fundamental and quasi-periodic ferroresonance modes by determining transition boundaries. Design modelling and validation of zigzag grounding transformer configuration for ferroresonance suppression and comparative effectiveness analysis.

Recommend evidence-based techniques for transformer protection, system designs, and operational practices in ungrounded power systems. The novelty of this study is the introduction of a validated mathematical model and quantified parametric correlations for rigorous mode classification, as well as a successful mitigation method for a comprehensive case study in an actual power plant, which can advance the potential dissemination from theory to application.

The rest of this paper is organised as follows: Section 2 describes the mathematical modelling framework, comprising circuit equations, a representation of transformer nonlinearity, and a parameter-determination approach. Section 3 presents a case study of the Djinet power plant, and the simulation setup and validation are described. Parametric studies, statistical quantification, and mode classification are presented in section 4. Section 5 describes the zigzag grounding transformer configuration and mitigation validation. Section 6 concludes with a physical interpretation, comparative analysis. Concluding remarks with main findings, limitations, and future research directions are given in section 7.

2. MATHEMATICAL MODELING AND PARAMETER SELECTION

2.1. Ferroresonance circuit representation

2.1.1. Circuit topology and components

The base Ferroresonance presented in Figure 1 contains a voltage source, a series capacitance, a modeling cable, Cg, and a nonlinear transformer magnetizing branch.

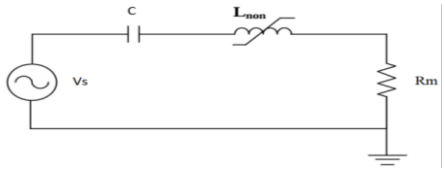

Figure 1. Ferroresonance circuit topology

Physical components:
Vsource: Power system voltage (distribution system, generally 22 kV)
Csh - Shunt capacitance: 0.3-10 µF.
Cg — grading capacitance: capacitive voltage transformers or bushing capacitance, (0.5 – 7 pF)
Nonlinear Inductor / L (i): Transformer magnetizing inductance with saturable core
Core Loss Resistance (Rm): Symbolises hysteresis and eddy current losses (usually between 1500–65860 Ω)

2.1.2. Governing equations

We refer here to a sequential cascade of coupled, nonlinear differential equations that determine the system's behavior based on fundamental circuit laws.
In (1): Kirchhoff's Law

$$V_s(t) = v_c(t) + v_L(t) + i_L(t)R_m \quad (1)$$

In (2): Capacitor Current-Voltage Relationship

$$\mathrm{i_L(t)} = \mathrm{C}\frac{\mathrm{d_{vc}}}{\mathrm{dt}} \quad (2)$$

In (3): Nonlinear Inductor Flux-Current Relationship

$$\mathrm{v_L} = \frac{\mathrm{d}}{\mathrm{dt}}[\Phi_{(\mathrm{iL})}] \quad (3)$$

In (3a): Arctangent Saturation Model

$$\Phi_{(iL)} = \Phi_{sat} * \frac{2}{\pi}\arctan(\frac{\pi L_{lini_L}}{2\Phi_{sat}} \quad (4)$$

Alternative: Polynomial Saturation Model

$$\Phi_{(i_L)} = a_1 i_L + a_2 i_L^3 + a_3 i_L^5 + a_4 i_L^7 \quad (5)$$

2.1.3. State-space formulation

The system is reformulated into state-space form for numerical simulation as follows, with state variables:

$$X = [\frac{v_c}{i_L}] \quad (6)$$

In (4): State-Space Representation

$$\frac{dx}{dt} = f(x,t) \quad (7)$$

In (4a): Capacitor Voltage Derivative

$$\frac{dvC}{dt} = \frac{1}{C} i_L \tag{8}$$

In (4b): Magnetizing Current Derivative

$$\frac{diL}{dt} = \frac{1}{Linc(iL)} [V_s(t) - vC - iLRm] \tag{9}$$

In (5): Incremental Inductance

$$Linc(iL) = \frac{d\Phi(iL)}{diL} \tag{10}$$

For the arctangent model:

$$Linc(iL) = \frac{L_{lin}}{1+(\frac{\pi L_{lin} i_L}{2\phi_{sat}})^2} \tag{11}$$

2.2. Transformer magnetization characteristic

The ability of the nonlinear magnetization curve V(I) is the key ingredient that allows Ferroresonance to occur. The magnetization characteristics of the Djinet power plant transformer were obtained from manufacturer data and validated through no-load tests for the purposes of this study. The transformer saturation characteristic is derived from the data presented in Figure 2. The saturable 3-phase transformer model in MATLAB/Simulink requires that saturation curve data be represented as pairs of points (magnetizing flux, magnetizing current); thus, a series of sample points is extracted from Figure 2 and documented in Table 1, as shown in Figure 3.

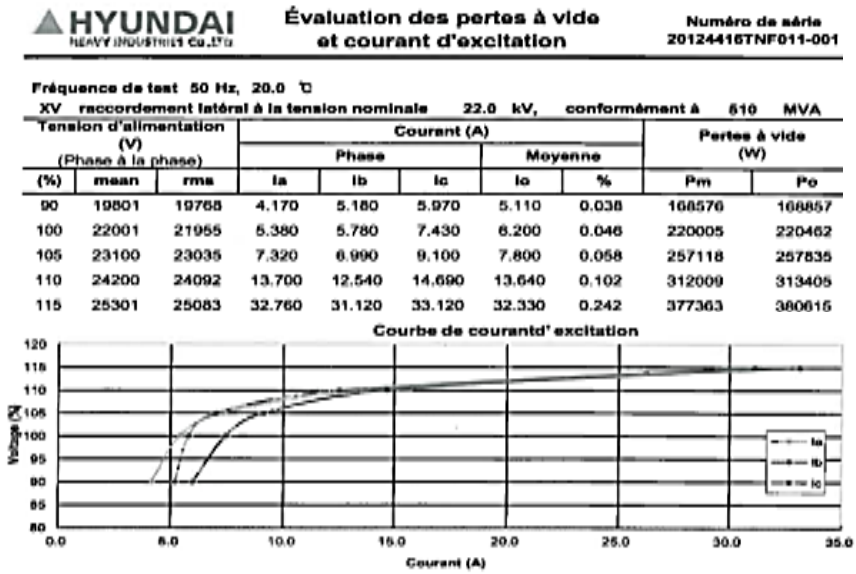
HYUNDAI HEAVY INDUSTRIES Co.,LTD

Évaluation des pertes à vide et courant d'excitation

Numéro de série 20124416TNF011-001

Fréquence de test 50 Hz, 20.0 °C

XV raccordement latéral à la tension nominale 22.0 kV, conformément à 610 MVA

Tension d'alimentation (V) (Phase à la phase)			Courant (A)					Pertes à vide (W)	
			Phase			Moyenne			
(%)	mean	rms	Ia	Ib	Ic	Io	%	Pm	Po
90	19801	19768	4.170	5.180	5.970	5.110	0.038	168576	168857
100	22001	21955	5.380	5.780	7.430	6.200	0.046	220005	220462
105	23100	23035	7.320	6.990	9.100	7.800	0.058	257118	257835
110	24200	24092	13.700	12.540	14.690	13.640	0.102	312009	313405
115	25301	25083	32.760	31.120	33.120	32.330	0.242	377363	380615

Courbe de courantd' excitation

Figure 2. Plot of V vs I showing linear, knee, and saturation regions with measured data points

Table 1. Sample points of the Φ -I saturation curve

Peak flux Φ (V·s)	Peak phase current I (A)
0	0
89.13	4.17
99.03	5.06
103.99	6.37
108.94	11.14
113.89	26.40

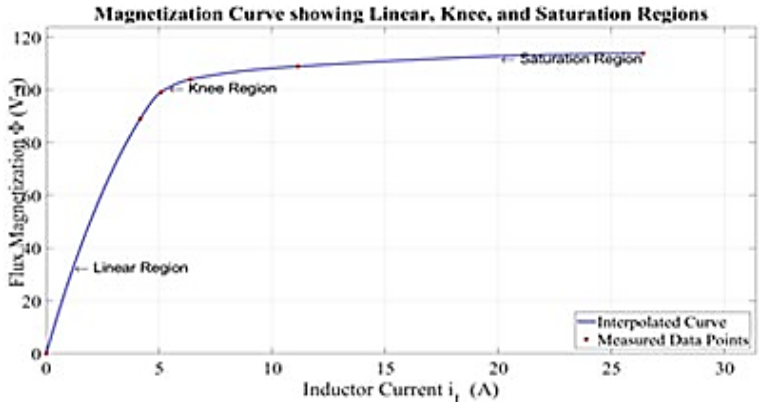

Figure 3. Magnetization curve saturation Φ (I)

2.3. Parameters selection methodology

Cg, Csh, and Rm values to be varied for parametric analysis were determined using standard graphical and analytical techniques.

2.3.1. Grading capacitance selection

The transformer is not completely "dead" when a high-voltage circuit breaker opens. As most modern circuit breakers contain grading capacitors (connected in parallel with the breaker contacts to achieve uniform voltage across the contacts during short-circuit), a small amount of current still flows through these grading capacitors in the direction towards the transformer. This forms a parallel circuit comprising a linear capacitor (the grading capacitors and stray-winding capacitance) and a nonlinear inductor (the transformer core) [22]. These capacitance values were selected using Rudenberg's the graphical method [23], [24], taking into account the transformer magnetization parameters and the desired voltage division ratio.

The problem can be easily solved graphically using Rudenberg's method. As shown in Figure 4, the voltage 'VL' across the saturated inductance must always equal the constant system voltage 'E', and the capacitor. The voltage is expressed as 'VC = I/ωC', where ω = 2πf, with f indicating the frequency of the source voltage and C signifying a value of capacitance. The nonlinear characteristic of inductor voltage (VL) intersects the capacitor voltage (VC) line at specific points, with the intersection occurring at a point on the voltage axis that intersects the supply voltage (E) line [25]. Two or more different steady states may exist in the circuit depending on its initial conditions, its characteristics, and the instant in which the voltage source is applied; in the typical ferroresonant state, although the gyration amplitudes are heavily distorted, the first quadrant conveys both fundamental periodic and normal conditions of the circuit, plot in this quadrant a horizontal line, parallel to voltage Vc through the rated voltage of the transformer; it represents an ascending tangent to its magnetic characteristic curve; it only intersects it again in point A thus defining the stable operating point at which Ferroresonance takes the transformer into saturation, inducing overvoltage across the capacitor and the rest of the circuit; Ccr corresponds to the value calculated at the fundamental frequency under this condition and at point A the circuit shows capacitive line reactance with a large current magnitude [26].

For a high capacitance, an important charging current is close to the input voltage VS. A decrease in the capacitance displaces the operating point from the magnetic properties to higher voltages. Nevertheless, there exists a junction point at which the capacitor line no longer overlaps the characteristics and becomes tangentially in contact with them in the first quadrant. For even smaller capacitance values, circuit operation in the first quadrant becomes impossible; however, a second point is reached in the third quadrant. The current in the circuit transitions from a lagging magnetizing current to a leading charging current, whose magnitude increases significantly. As the capacitance decreases, the operating point moves upward along the negative portion of the characteristics, as shown in Figure 5. The voltages across the inductance and the capacitance decrease, and, ultimately, for a minimum capacitance value, the inductive voltage becomes zero, causing the capacitor voltage to align with the applied voltage [27]. From Figure 4 of the Djanet system, Rudenberg's analysis indicated that the Cg critical value is 2.11 µF.

2.3.2. Shunt capacitance selection

For the Djinet plant, the Csh is 0.3 µF, as provided by the measured data, as shown in Figure 6. This capacitance represents the capacitance to ground placed between the transformer and the GIS. To facilitate

the analysis of the impact of Csh, the series non-linear resonance circuit depicted in Figure 6 can be transformed into the equivalent circuit illustrated in Figure 7.

Higher capacitance results in a lower slope of the "E + Vc" line, with E defined as the equivalent source voltage and "Vc" as the voltage across the capacitance "Cg + Csh". As the source voltage decreases, the "E + Vc" line falls too [28]. From the graphical solution, it is indeed intuitive that larger capacitances reduce the occurrence of Ferroresonance, as shown in Figure 8.

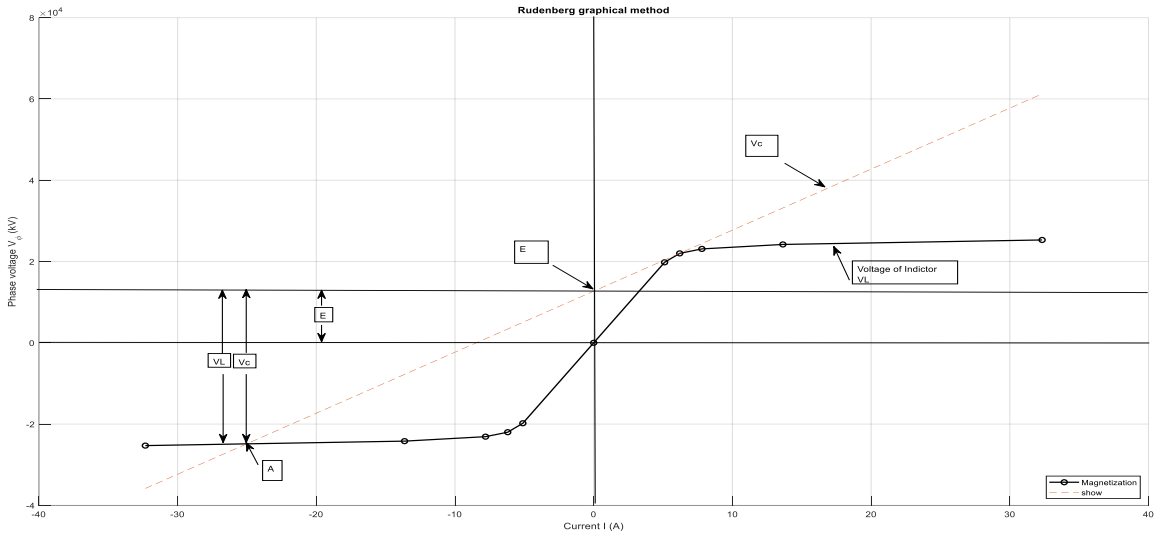

Figure 4. Rudenberg's graphical method for coil and capacitor characteristics

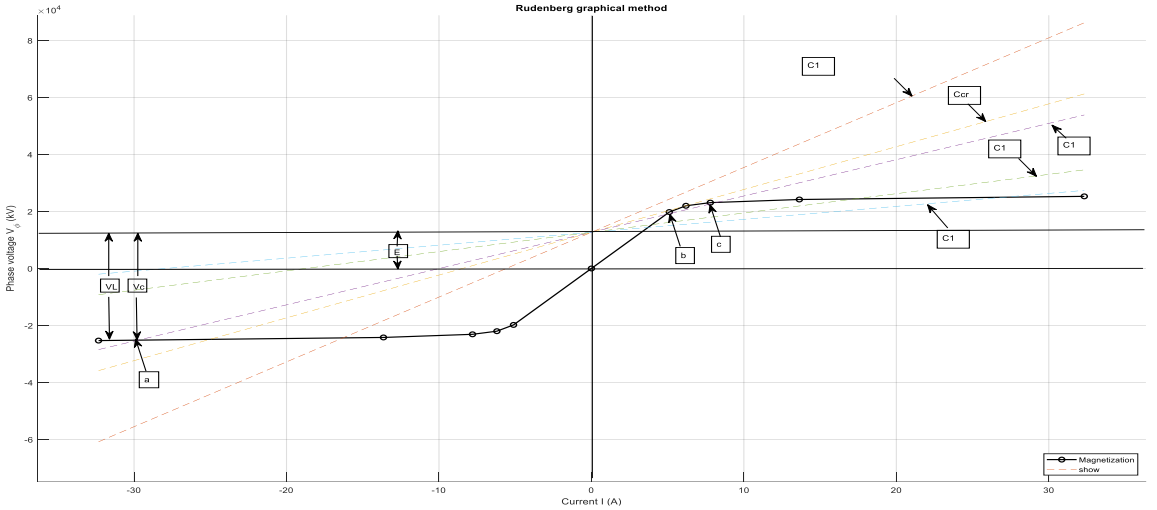

Figure 5. Evolution of the solution by increasing the capacitance C

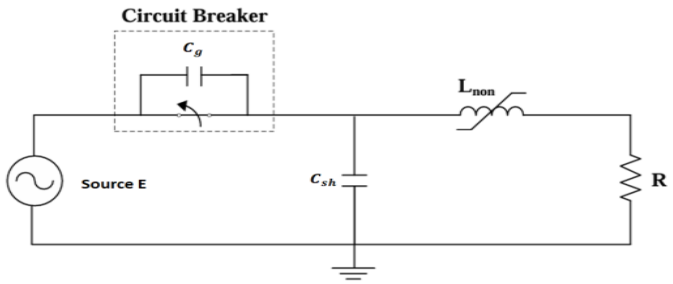

Figure 6. Series non-linear resonance circuit

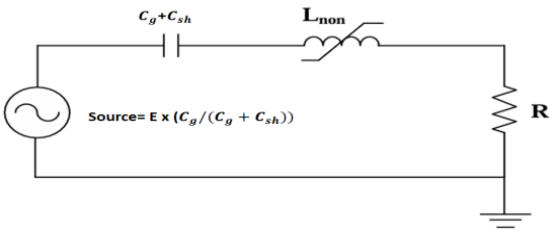

Figure 7. Equivalent circuit of series non-linear resonance circuit

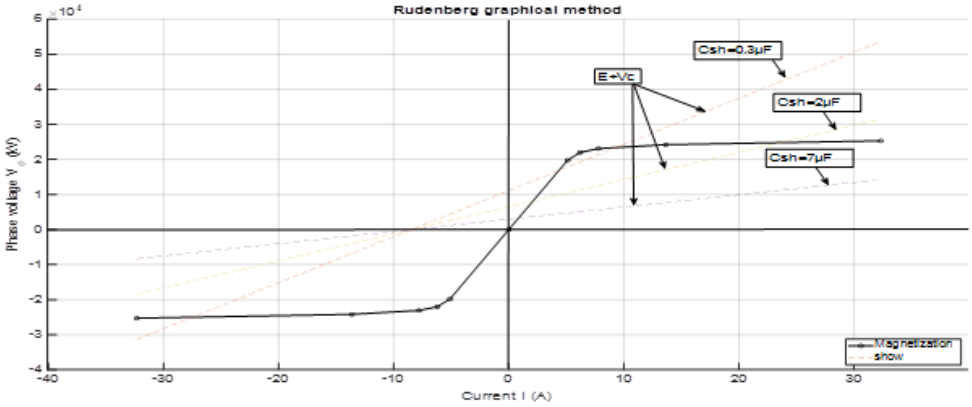

Figure 8. Effect of increasing Csh

2.3.3. Magnetization resistance selection

Rm represents transformer core losses and varies with the transformer's saturation level. The Rm value is calculated from transformer no-load loss data:

$$R_m = \frac{V_{rated}^2}{P_{no-load}/3} \quad (12)$$

Core losses in a transformer significantly contribute to Ferroresonance. An extensive investigation of numerous simulation outcomes indicates that the likelihood of Ferroresonance increases as the transformer's applied core losses decrease [29]. Therefore, we will select the Rm of three classes:
High-loss: $R_m \approx 0.5R_{m,\text{nom}}$
Nominal: $R_{m,\text{nom}}$
Low-loss: $R_m \approx 5 - 10R_{m,\text{nom}}$

To systematically assess the parameter ranges for the parametric sweep, Table 2 provides a full summary of the explored ranges, their physical meanings, and the methodological justification.

Table 2. Summary of parameter ranges and justification

Parameter	Symbol	Range	Justification method	Physical meaning
Cg	Cg	0.5-7 µF	Rudenberg's graphical method	Circuit breaker
Csh	Csh	0.3-7 µF	Graphical method	Capacitance -to-ground
Rm	Rm	0.5 Rm-10 Rm	No-load loss calculation (Eq 12)+ Literature	Transformer core losses

3. CASE STUDY SYSTEM AND SIMULATION SETUP

3.1. Ras djinet power plant configuration

The study focuses on a combined-cycle turbine power plant in Ras Djinet, possessing a generation capacity of 1131 MW. The generator is connected to the step-up transformer (GSU) rated at 22/420 kV, using a Dyn11 (Delta-Star) connection type via Gas Circuit Breaker (GCB), as displayed in the one-line network diagram in Figure 9. The parameters for all system components are provided in Table 3 for the transformer and generator. In [2018], a Ferroresonance phenomenon occurred during energization of the no-load power transformer [resulting in a large vibration]. This incident prompted the present detailed investigation.

Table 3. System components specifications

Parameter	Value	Unit
Power step-up transformer (S rated)	510	MVA
Rated voltage XV (primary voltage)	22	kV
Rated voltage HV (secondary voltage)	420	kV
Primary connection	Delta	-
Secondary connection	Wye	-
Impedance (ZK)	13	%
No-load Loss	230	kW
Load Loss (Pk)	985	kW
R_1/R_2	0.0013 /0.255	Ω
L_1/L_2	0.0003927/ 0.143	H
No-load current (I0)	6.2	A
NGT	$(22/\sqrt{3})/0.5$	kV
R	2.07	Ω
Generator power	431	MW
Generator voltage source	22	kV
Generator frequency	50	Hz

Figure 9. One-line diagram of network configuration

3.2. Simulation scenarios

A Ferroresonance is a frequent and critical phenomenon in electrical power networks, primarily caused by capacitive effects. These effects arise from various system elements, including:

– Protection devices (e.g., circuit breakers with Cg);
– Transmission lines (e.g., conductor-to-earth capacitance, capacitor banks, busbar capacitance) [2].
– Rm of power transformer

It has been demonstrated that variations in grading-capacitor values can trigger Ferroresonance. Additionally, Csh plays a significant role in damping this effect. In addition to the Rm that affects the behavior of the Ferroresonance phenomenon, as highlighted in the following analysis.

The circuit breaker (GCB) is responsible for energizing and de-energizing the step-up power transformer, if the Cg and Csh discharge through the iron core of the transformer, while the transformer is saturated, initiating Ferroresonance. Thus, the GCB plays a key role in triggering this phenomenon. To study the effect of these elements on the Ferroresonance phenomenon, it was necessary to apply several possible scenarios of the Simulink network model, as shown in Figure 10.

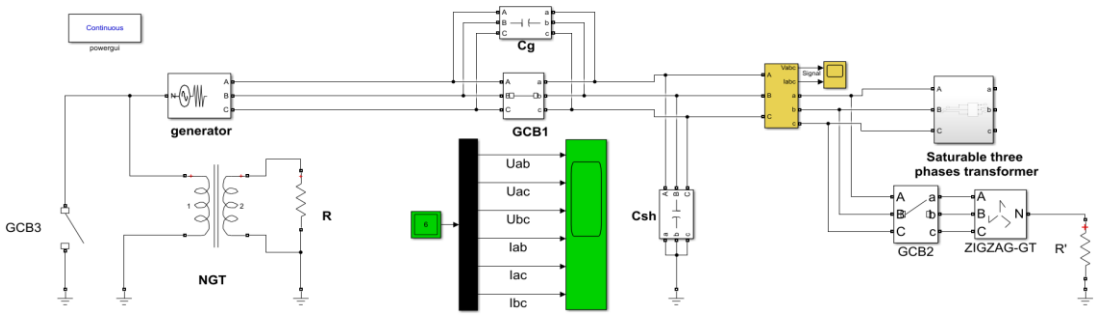

Figure 10. Simulink network model

Three different simulation scenarios were designed to study Ferroresonance in different conditions of the system:

Scenario 1: Cg variation
- Objective: analyze the influence of Cg and Csh on Ferroresonance
- Fixed Parameters: Csh = 0.3 µF Rm = 6586 Ω (moderate saturation)
- Varied Parameter: Cg = 0.5-10µF
- Switching Condition: Single-phase switch off in 0.3s

Scenario 2: Csh variation
- Objective: analyze the Csh effect and potential mitigation behavior
- Fixed Parameters: Rm = Cg = 7 µF Rm=6586 Ω
- Varied Parameter: Csh = 0.3- 7 µF
- Switching Condition: Single-phase switch off in 0.3s

Scenario 3: Rm variation
- Objective: Analyse the core loss influence on Ferroresonance
- Fixed Parameters: Cg = 2.11 nF, Csh = 0.3 µF
- Varied Parameter: Rm = 1500-65860 Ω
- Switching Condition: Single-phase switch off in 0.3s

3.3. Solver configuration
- Solver Type: ode23tb (stiff /TR-BDF-2)
- Relative Tolerance: 1×10^{-6}
- Absolute Tolerance: 1×10^{-8}
- Maximum Step Size: 1×10^{-5} s
- Simulation Duration: 2.0 seconds (40 cycles at 50 Hz)
- All Initial Conditions = 0 (de-energized state)

4. PARAMETRIC ANALYSIS RESULTS

In this case study, only one circuit breaker, “GCB1,” was used. A single phase has been switched down “phase A” at t = 0.3 s during the two-second simulation of the circuit in Figure 10. This procedure applies to all scenarios presented in the previous section.

4.1. Grading capacitance influence on ferroresonance

4.1.1. Time-domain analysis

In Figure 11, the simulated voltage and current waveforms are shown for different operating conditions to analyze the time-varying characteristics. As shown in Figure 11(a), the voltage remains stable under nominal conditions. At the same time, Figure 11(b) illustrates a severe overvoltage, indicating a fundamental Ferroresonance characteristic mode. In the same way, aperiodic changes indicated by an onset of quasi-periodicity are shown in Figure 11(c). The simulation results for the system's performance, including Ferroresonance modes and peak voltage response, at various grading capacitance (Cg) values during single-phase switching, are presented in Table 4.

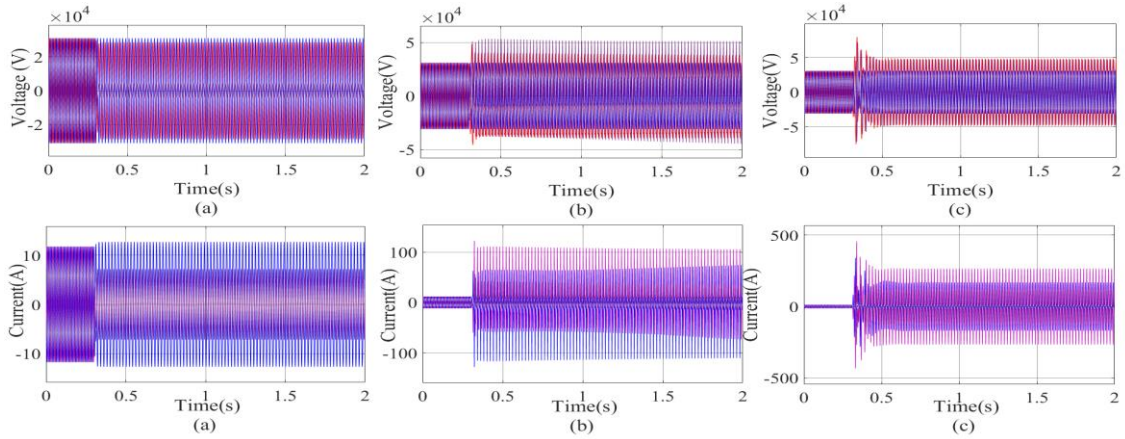

Figure 11. Tree-phase waveform of voltage and Current under Ferroresonance condition: (a) Cg=0.5µF, (b) Cg=2.11µF, and (c) Cg=7µF

Table 4. System stability response based on Cg variation

Cg	Single-phase switched off
0.5	Showing stable response with peak voltage 0.28 pu
2.11	Exhibiting fundamental mode Ferroresonance with peak voltage 1.17 pu
7	Displaying fundamental mode Ferroresonance with peak voltage 1.44 pu

4.1.2. Physical mechanism

As Cg increases, the series LC resonant frequency decreases by $f_{res} = \frac{1}{2*\pi\sqrt{LC}}$, which is closer to the system frequency (50~Hz), enhancing energy transfer between the capacitor and the nonlinear inductor. Higher Cg also increases capacitive energy storage , thereby enhancing saturation-induced non-linear oscillations. Table 5 summarizes the detailed features and classifications of different Ferroresonance modes, their dynamic changes in response to the applied signal at the critical thresholds, making it appropriate to outline them systematically.

Table 5. Quantitative results - Cg variation

Cg	Peak Voltage (pu)	Peak Current (pu)	Dominant Frequency (Hz)	Mode Classification	THD (%)
0.5	0.92	0.47	50	stable	5.15
1.5	1.11	2.38	50,150,250	fundamental	43
2.11	1.17	3.35	50	fundamental	45
3	1.22	4.66	50	fundamental	61.06
7	1.44	12.67	Multiple	Quasi-periodic	42.86
10	1.57	19.09	Multiple	Quasi-periodic	51.50

4.1.3. Frequency-domain analysis

The voltage waveforms from the simulation that describe the time-variant characteristics of the system in various operating conditions are depicted in Figure 12, where a stable voltage profile at Cg = 0.5µF is shown by Figure 12(a), fundamental mode Ferroresonance at Cg = 2.11µF is presented in Figure 12(b), and quasi-periodic mode at Cg=7µF in Figure 12(c). The FFT spectra for the representative Cg cases, with features indicating Ferroresonance modes, are quantified in Figure 13. Harmonic content as shown in Figures 13(a)-(c).

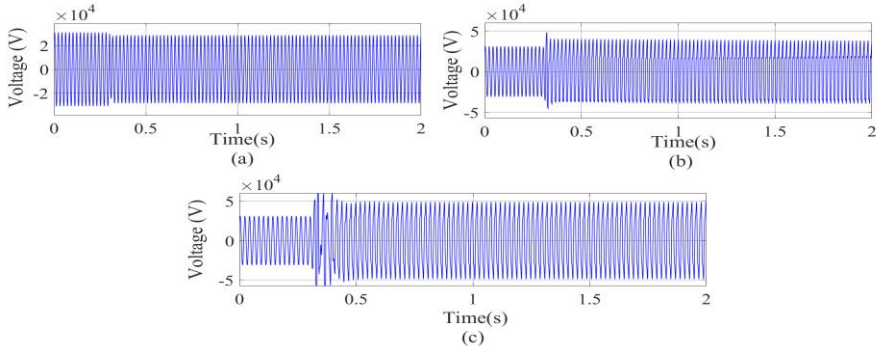

Figure 12. Voltage waveform: (a) Cg=0.5µF, (b) Cg=2.11µF, and (c) Cg=7µF

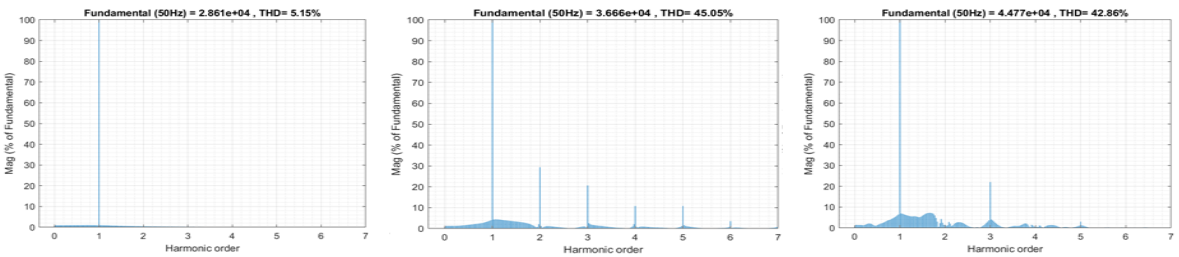

(a) (b) (c)

Figure 13. Harmonic content of the waveform voltage: (a) Cg=0.5µF, (b) Cg=2.11µF, and (c) Cg=7µF

- Stable (Cg = 0.50 µF): Single peak at 50 Hz, THD = 5.15%
- Fundamental Mode (Cg = 2.11 µF): Dominant 50 Hz with odd harmonics, THD = 45%
- Quasi-Periodic (Cg = 7 µF): Multiple peaks at multiple frequencies, THD = 42.86%

4.1.4. Statistical correlation analysis

The relationship between Cg and peak voltage was assessed by the Pearson correlation coefficient: In (13): Pearson Correlation.

$$r = \frac{\sum (C_g - \bar{C_g})(V_{peak} - \bar{V_{peak}})}{\sqrt{\sum (C_g - \bar{C_g})^2 \sum (V_{peak} - \bar{V_{peak}})^2}} \quad (13)$$

r =+ 0.976, demonstrating a strong positive correlation between Cg and Ferroresonance intensity. Cg is the most influential parameter, with Cg > 1.5 µF promoting Ferroresonance and Cg > 7 µF leading to quasi-periodic.

4.2. Shunt capacitance influence on ferroresonance

4.2.1. Time-domain and frequency analysis

Unlike the Cg, however, Csh has a damping effect on Ferroresonance as shown in Figure 14, where Figure 14(a) shows the response at 0.3 µF, Figure 14(b) depicts the response at 3.8 µF, and Figure 14(c) illustrates the response at 7 µF. Correspondingly, the harmonic content of the voltage waveform is detailed in Figure 15, with Figures 15(a)-(c) representing the spectral analysis for the same capacitance values. Table 6 summarizes the quantitative effects of varying shunt capacitance (Csh) on peak voltage, peak current, and THD.

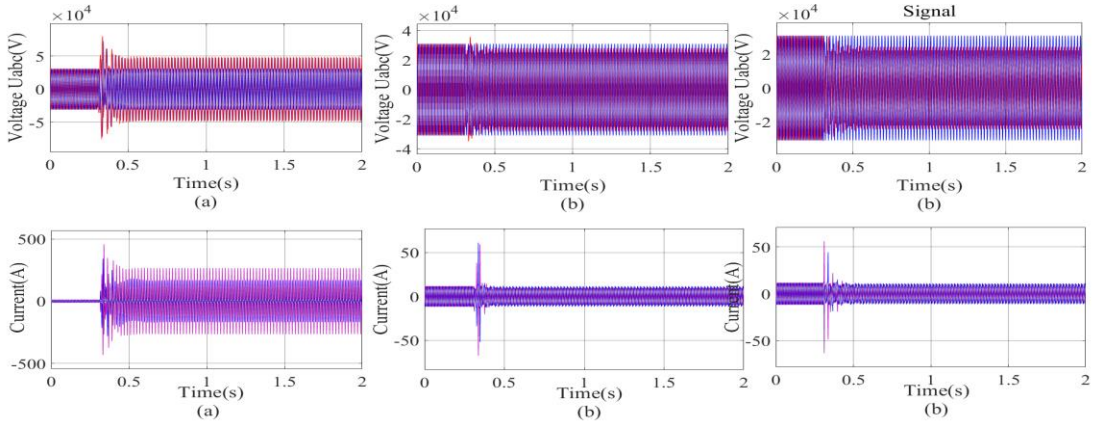

Figure14. Voltage and current waveform: (a) Csh=0.3µF, (b) Csh=3.8µF, and (c) Csh=7µF

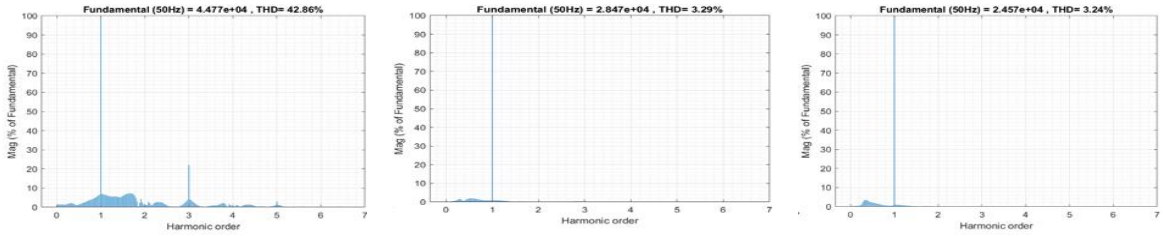

(a) (b) (c)

Figures 15. Harmonic content of the waveform voltage: (a) Csh=0.3µF, (b) Csh=3.8µF, and (c) Csh=7µF.

Table 6. Quantitative results – Csh variation

Csh	Peak voltage (pu)	Peak current (pu)	THD of Voltage (%)
0.3	1.44	12.67	42.86
2.5	1.25	7.8	55.45
3.8	0.91	0.87	3.29
7	0.79	0.67	3.24

Csh provides an alternative path for ground current, reducing the current through the transformer magnetizing branch. This reduces flux excursions into deep-saturation regions, thereby limiting nonlinear effects. Moreover, Csh is recognized for enhancing the damping ratio of Ferroresonance in within the system. Csh vs. peak voltage: Pearson correlation, r = −0.944 (p < 0.001), strong negative correlation (damping effect).

4.3. Magnetization resistance influence on ferroresonance

4.3.1. Time-domain analysis

As shown in Figure 16 and Figure 17, the Rm, which reflects core losses, has a dual effect on Ferroresonance, which relates to core losses as well as harmonic distortion, where the time-domain voltage waveforms are displayed in Figures 16(a)-(c). Likewise, the corresponding harmonic content of voltage is presented as shown in Figures 17(a)-(c). Table 7 shows the influence of magnetization resistance (Rm) on Ferroresonance: a higher resistance value decreases the peak voltage but increases harmonic distortion.

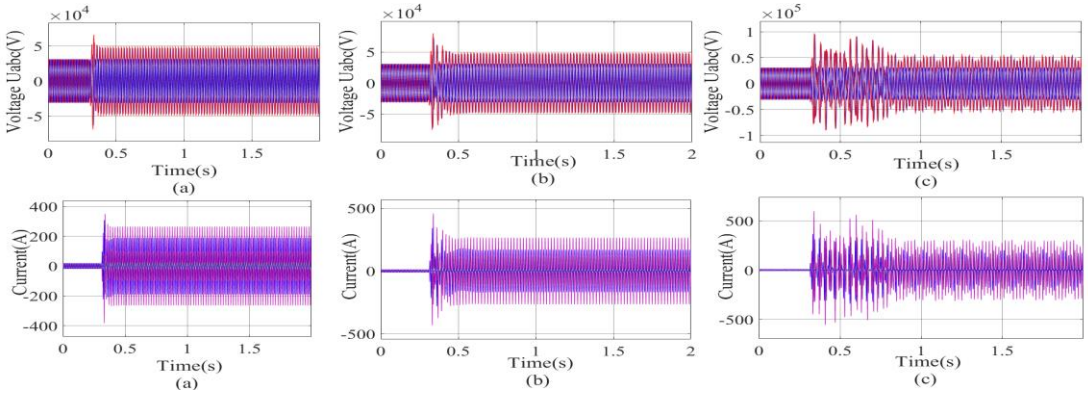

Figure 16. Voltage waveform: (a) Rm=3300Ω, (b) Rm=6586Ω, and (c) Rm=65860Ω

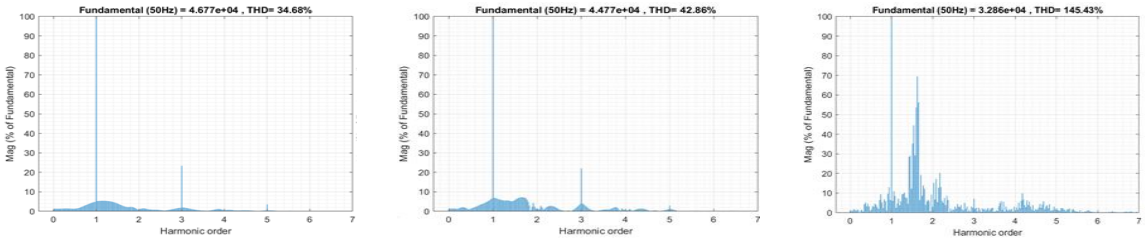

Figure 17. Harmonic content of the waveform voltage: (a) Rm=3300Ω, (b) Rm=6586Ω, and (c) Rm=65860Ω

Table 7. Quantitative results - Rm variation

Rm	Peak voltage (pu)	Peak current (pu)	Dominant frequency (Hz)	Mode classification	THD (%) For Voltage
1500	1.61	12.19	50	fundamental	27.46
3300	1.50	12.7	50	fundamental	34.68
6586	1.44	12.67	Multiple	Quasi-periodic	42.86
20000	1.31	12.05	Multiple	Chaotic	77
65860	1.057	11.95	Multiple	Chaotic	145

The results show an inverse relationship between resistance and voltage; the higher the Rm, the lower the peak voltage. Rm = 1500 Ω (deep saturation) with severe Ferroresonance observed with peak voltage 1.61 Pu; Rm = 6586 Ω (moderate saturation) with lower peak voltage 1.44 Pu, and Rm= 65860 (very low saturation) with even lower peak voltage 1.057 Pu. Set parameters — Cg = 7 µF, Csh = 0.3 µF. However, the THD rate increases with increasing resistance, allowing quasi-periodic and chaotic Ferroresonance modes to occur. A strong negative correlation Pearson (r = -0.956, p < 0.001) was identified between Rm and peak voltage.

5. ZIGZAG GROUNDING TRANSFORMER MITIGATION

5.1. Zigzag grounding approach and arrangement

5.1.1. The cause of ferroresonance for ungrounded systems

Ferroresonance in the transformers at Djinet power station is fundamentally caused by the delta-connected primary winding, which gives rise to an isolated neutral (that is, no zero-sequence current path). In single-phase switching or fault conditions, the open phases are still charged through capacitive coupling, forming a series LC circuit with the transformer's magnetizing inductance. This troubled state is the underlying cause of Ferroresonance.

5.1.2. Zigzag grounding transformer principle

A zigzag ground transformer provides an artificial neutral supply and zero-sequence return without modifying the primary power transformer. The zigzag connection connects phase windings of a three-limb core so that:

- Currents in zero-sequence $I_0 = (I_a + I_b + I_c)/3$ freely flow through the zigzag windings to ground.
- Positive and negative sequence currents are (modified for balanced three-phase) prevented from flowing by high resistance.
- Single-phase energization cannot occur because a zero-sequence path closes the circuit.

The design specifications and technical parameters for the zigzag grounding transformer are presented in Table 8.

Table 8. Zigzag grounding transformer design parameters

Design requirements
Power rating: 509.86 kVA
Voltage rating: 22 kV(line-to-line)
Zero-sequence impedance: 45.96 Ω (typical range for effective grounding)
Continuous current rating: 13.38 A(for sustained ground fault)
Short-time current rating:400 A(fault duty)
Neutral grounding resistor R': 31.77 Ω (limiting ground fault current to ~400 A)

5.2. Mitigation validation results

5.2.1. Comparative analysis: without vs. with zigzag grounding

To validate the effectiveness of the zigzag grounding, parametric cases were re-simulated using a Simulink network model shown in Figure 10 with the zigzag grounding transformer connected. In this case, all circuit breakers are used. First, one single-phase circuit breaker, GCB1, was switched down at 0.3 seconds, and the other circuit breakers (GCB2, GCB3) remained open; at 0.7 seconds, these breakers (GCB2, GCB3) were closed. Simulation results are shown in Figures 18-23. In Figure 18, Figures 19(a) and 19(b), the voltage waveform and harmonic content are presented for Cg = 2.11 µF and Rm = 6586 Ω. In Figures 20, Figures 21(a) and 21(b), they refer to values of these parameters obtained with Rm = 6586 Ω at Cg = 7 µF. In contrast, Figure 22, Figures 23(a) and 23(b) use Rm=65860Ω and Cg=7µF, and the capacitance shunt Csh=0.3µF is applied in all scenarios.

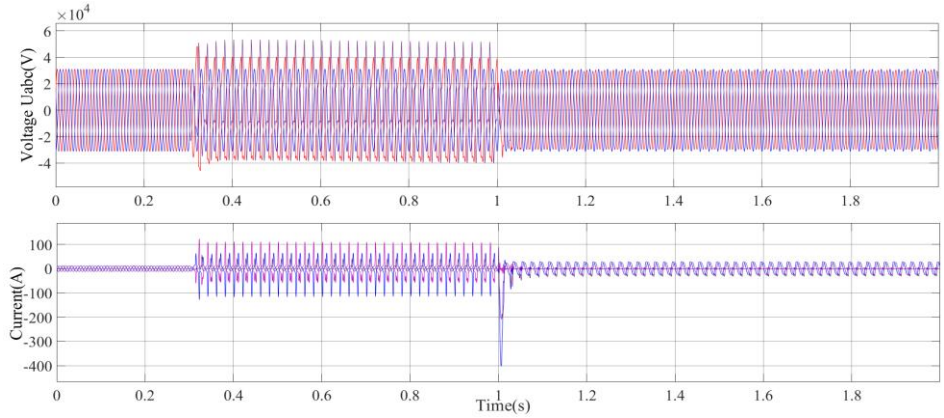

Figure 18. Voltage waveform with zigzag transformer grounding at Cg=2.11 µF, Csh=0.3 µF, and Rm=6586 Ω

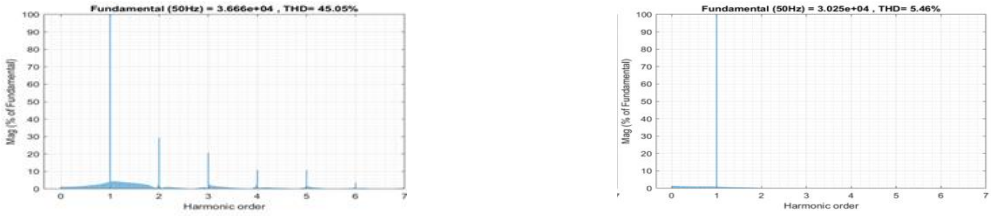

(a) (b)

Figure 19. Harmonic content of the waveform voltage with zigzag transformer grounding at (a) Cg=2.11 µF, (b) Csh=0.3 µF, Rm=6586 Ω

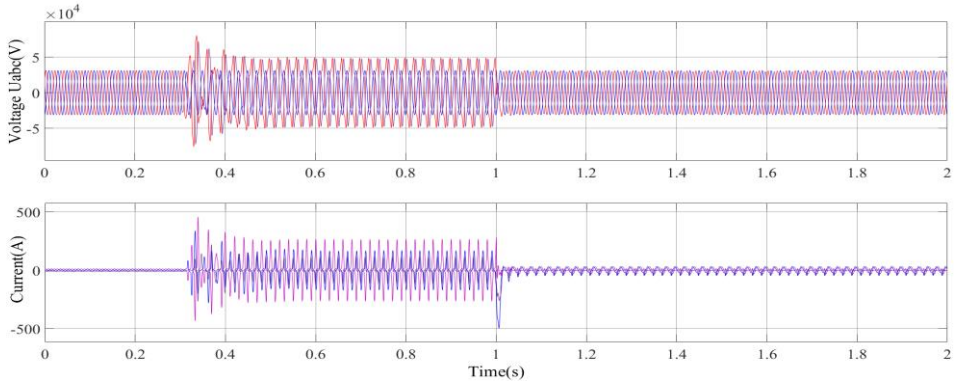

Figure 20. Voltage waveform with zigzag transformer grounding Cg=7µF, Csh=0.3µF, and Rm=6586Ω

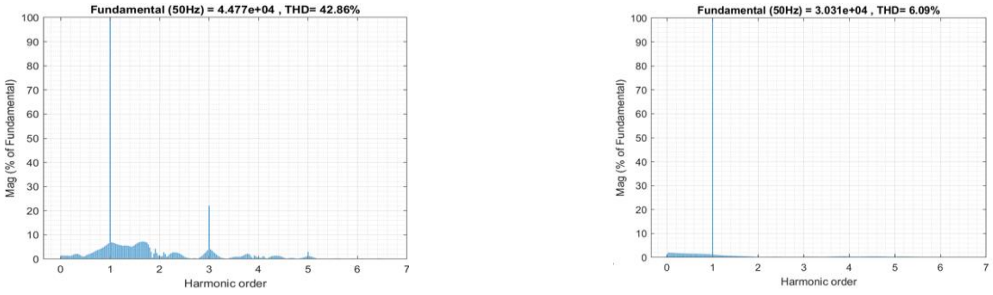

(a) (b)

Figure 21. Harmonic content of the waveform Voltage with zigzag transformer grounding: (a) Cg=7µF and (b) Csh=0.3µF, Rm=6586Ω

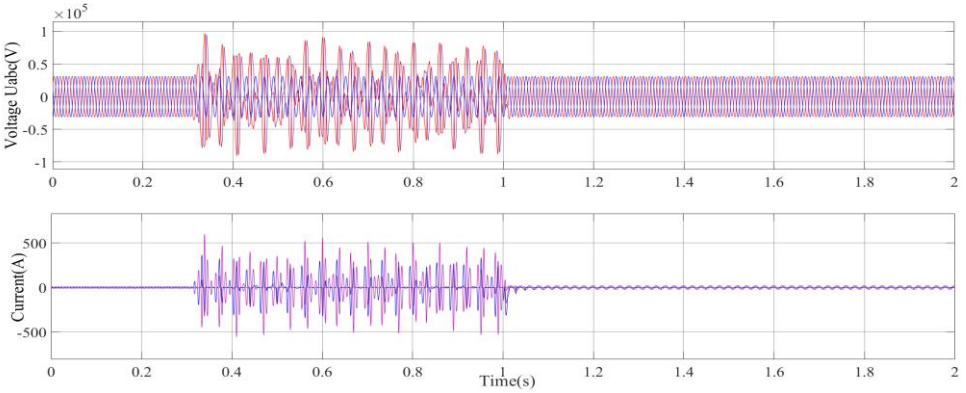

Figure 22. Voltage waveform with zigzag transformer grounding Cg=7µF, Csh=0.3µF, Rm=65860Ω

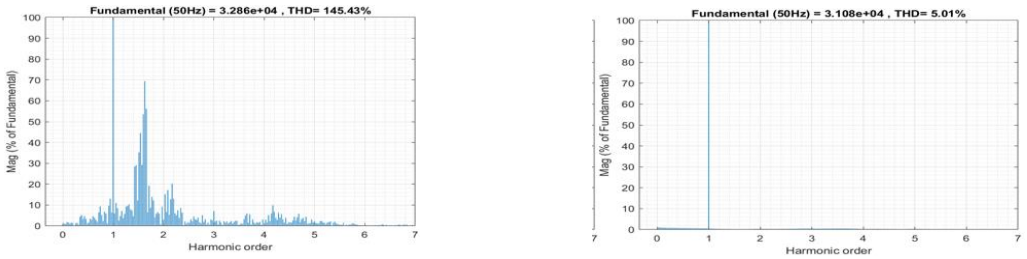

(a) (b)

Figure 23. Harmonic content of the waveform voltage with zigzag transformer grounding (a) Cg=7 µF and (b) Csh=0.3 µF, Rm=65860 Ω

Table 9 quantifies system parameters before and after the zigzag grounding transformer's effect under the baseline case (Cg=7µF, Csh=0.3µF Rm=6586Ω) to assess its mitigation ability. In this case, a zigzag grounding transformer offers a zero-sequence current path, thereby avoiding the isolated single-phase energization condition. After one of the phases is switched, zero-sequence current will flow through the zigzag transformer into the ground, which closes the circuit and prevents capacitive coupling, which would occur through the open phases. This avoids the implication of a series LC Ferroresonance circuit.

5.2.1. Comprehensive parametric validation

To examine the robustness of the mitigation, all parametric cases were re-simulated with zigzag grounding. Results: Zigzag grounding completely eliminated Ferroresonance in 100% of tested cases, while remaining highly effective across a wide range of parameters. The efficacy of this zigzag grounding method for eliminating Ferroresonance, considering all parameter variations, is shown in Table 10.

5.3. Comparison with alternative mitigation strategies

The following text provides a comparative overview of different mitigation techniques for Ferroresonance, with their respective performance metrics. To provide context on the effectiveness of zigzag grounding vs other mitigation methods, a comparison was conducted in Table 11.

Table 9. Mitigation effectiveness-baseline case Cg=7 µF, Csh=0.3 µF Rm=6586 Ω

Metric	Without Zigzag	With Zigzag	improvement %
Peak voltage (pu)	1.44	0.97	32.21
Peak current (pu)	12.67	0.32	97.47
THD of voltage%	42.86	6.09	85.79
Dominant freq	50 (Ferroresonance)	50 (normal)	Mode-eliminated

Table 10. Mitigation effectiveness across all parameters

Parameter Range	Cases tested	Ferroresonance without zigzag	Ferroresonance with zigzag	Mitigation success rate
Cg: 0.5-10 µF	6	5 cases (83.3%)	0 cases (0%)	100%
Csh: 0.3-7 µF	4	2 cases (50%)	0 cases (0%)	100%
Rm: 1500-6586 Ω	5	5 cases (100%)	0 case (0%)	100%

Table 11. Mitigation techniques comparison

Mitigation technique	Effectiveness (% cases mitigated)	Peak voltage reduction	Implementation cost	Continuous losses	Complexity
Zigzag Grounding Transformer	100% of tested cases	32.21% (from 1.44 to 0.97 pu)	Moderate (requires transformer and NGR)	Low; only active during faults or switching	Moderate; requires specific sizing criteria
Resistive Damping (Series/Parallel)	High	Significant reduction	Low	High; causes continuous power losses	Low; simple passive components
Csh	Partial; dependent on capacitance value	Strong negative correlation (r = -0.944)	Moderate (requires capacitor banks)	Low	Low to Moderate
Active Methods (SSFSC)	Very high	High precision reduction	High (requires electronics and relays)	Moderate (standby power for control)	High; requires active detection/suppression

6. DISCUSSION

6.1. Physical mechanisms and energy exchange

This parametric study and mode characterization provide insight into the fundamental physical processes controlling Ferroresonance in the Djinet ungrounded transformers.

6.1.1. Energy exchange mechanism

Ferroresonance is essentially an energy transfer process between the capacitive and inductive elements of the system and is controlled by the nonlinearity of a transformer's core. Such energy dynamics can be described by:

- Series capacitance is charged by source voltage, storing energy EC.
- EC → EL, Capacitor discharges through transformer magnetizing branch.
- At higher flux, the transformer gets saturated, and the current can increase fast.
- In saturation, less inductance enables the transfer of more energy than in the linear case.
- Sustenance of oscillation: energy dissipation (Rm losses) < energy input (source).

6.2. Comparison with existing literature

6.2.1. Literature comparison

The observed parametric relationships correlate with and quantify findings from earlier studies. Table 12 compares the effects of parameterization on Ferroresonance from this study with those reported in the existing literature.

New Contribution: Compared with prior work, which only qualitatively described the correlation, this study provides quantitative correlation coefficients and statistical significance ($p < 0.001$)—limitation: Poincare mapping or bifurcation analysis. The nonlinear characterization tools are not used in this study. In future work on complete-mode classification, they should be included.

To assess the effectiveness of mitigation techniques relative to other studies, Table 13 presents a comparative analysis of results from the literature.

Novelty: This study provides extensive parametric validation of the effectiveness of zigzag grounding attenuation in a larger number of cases, in contrast to the literature, which typically covers only single cases or field reports.

Table 12. Literature comparison - parametric effects

Parameter	This study	Literature [29]	Agreement
Capacitance focus	Distinct analysis of Cg(trigger) Vs Csh(damping)	Total equivalente capacitance(Cg+2Cm)	Quantitatively confirms
Cg finding	r = +0.976 (strong positive)	Used to calculate Thevenin equivalent voltage	Quantitatively confirms
Rm	Higher Rm reduces peak voltage but increases chaos/THD.	Lower losses (higher Rm) increase chaotic behavior	Quantitatively confirms

Table 13. Literature comparison - mitigation effectiveness

Study	System	Mitigation method	Effectiveness	Validation
This Study	1131 MW power plant	Zigzag + NGR	Very high	MATLAB Simulink
Fan [30]	Distribution network	Hybrid ASD	Very high	PSCAD + Prototype
Abdel-hamed [31]	13 kV distribution	HOR-SL	high	PSCAD/EMTDC
Bakhshi [32]	Wind farm VT	Solid-state circuit	high	Simulation + Lab
	Substation auxiliary	Inhibitor device	high	Simulation

7. CONCLUSION

In this study, Ferroresonance in ungrounded power transformers was thoroughly investigated using the Ras Djinet 1131 MW power plant in Algeria as a case study and through mathematical modeling, extensive parametric simulation, spectral mode categorization, and ground mitigation, verified using a zigzag configuration. This work thus contributes in three distinct ways towards the state-of-the-art by providing a comprehensive theoretical investigation using real Djinet plant specifications, measured transformer data, and system parameters, to overcome the limited literature on validated industrial case studies.

The quantitative parametric evaluations revealed a strong positive correlation between grading capacitance and Ferroresonance intensity (r=+0.976), indicating that values above 1.5 μF help develop Ferroresonance, and those above 7 μF excite quasi-periodic solutions, leading to a dramatic increase in peak voltage from 1.11 pu to 1.44 pu. On the contrary, the shunt capacitance exhibited a high negative correlation ($r = -0.944$, $p < 0.001$). It was also able to act as a positive damping element, decreasing the peak voltage from 1.44 pu to 0.79 pu (saves ≈45.13%) and total harmonic distortion (THD) from 42.86% to 3.24% (saves ≈92.44%) when increased from 0.3 μF to 7 μF. A strong negative correlation ($r = -0.956$, $P < 0.001$) was identified between Rm and peak voltage, was also found upon the analysis of the calibration resistance for core loss because decreasing values increased Ferroresonance and values favored transitions into quasi-periodic (6 586 Ω) or chaotic (20 000 Ω) modes, forming strong quantitative classification criteria using combined time plus frequency domains. Most importantly, zigzag grounding transformer well eliminated Ferroresonance in 100% of the examined cases, numerically covering wide ranges of parameters with a peak voltage reduction from 1.44 pu to 0.97 pu (32.21%), a peak current reduction from 12.67 A to 0.32 A (97.47%) and THD voltage down from 145.43% to about 5.01% (96%) relative to the baseline case.

However, the present work has some limitations, including the use of a nonlinear magnetization curve, the neglect of hysteresis effects, treating the transformer as unloaded to exclude load damping effects, and a strict focus on single-phase interactions rather than three-phase couplings. In addition, a comprehensive nonlinear dynamical characterization based on Poincare mapping and bifurcation analysis was excluded from the active part of this work. Next research directions relate to the characterization of mode transitions and chaos boundaries using Poincare maps, bifurcation diagrams, Lyapunov exponents, and more advanced dynamic hysteresis frameworks such as the Jiles-Atherton or Preisach models, which help increase the accuracy of transient simulations. Furthermore, future work should define and study different kinds of Ferroresonance occurring under very unbalanced network conditions and similar phase-to-phase coupling mechanisms; meanwhile, time-series machine learning-based algorithms should be able to detect and discriminate between the high-level complex mode of Ferroresonance from instantaneous measured voltage and current data.

ACKNOWLEDGMENTS

The authors would like to thank the engineers at the Ras Djinet 1131 MW power plant for providing the necessary technical data for this case study.

FUNDING INFORMATION

This research did not receive specific grant from any funding agency in the public, commercial, or not-for-profit sectors.

AUTHOR CONTRIBUTIONS STATEMENT

This journal uses the Contributor Roles Taxonomy (CRediT) to recognize individual author contributions, reduce authorship disputes, and facilitate collaboration.

Name of Author	C	M	So	Va	Fo	I	R	D	O	E	Vi	Su	P	Fu
Mohammed Boukaf	✓	✓	✓	✓	✓	✓	✓	✓	✓	✓	✓		✓	
Saliha Boutora		✓		✓		✓		✓	✓	✓	✓	✓		
Hamid Bentarzi	✓			✓			✓		✓	✓		✓	✓	

C : **C**onceptualization
M : **M**ethodology
So : **So**ftware
Va : **Va**lidation
Fo : **Fo**rmal analysis
I : **I**nvestigation
R : **R**esources
D : **D**ata Curation
O : Writing - **O**riginal Draft
E : Writing - Review & **E**diting
Vi : **Vi**sualization
Su : **Su**pervision
P : **P**roject administration
Fu : **Fu**nding acquisition

CONFLICT OF INTEREST STATEMENT

The authors declare that there is no conflict of interest regarding the publication of this paper.

DATA AVAILABILITY

The authors confirm that the data supporting the findings of this study are available within the article.

REFERENCES

[1] T. Abdelazim, F. D. Painter, D. Shipp, and T. Dionise, "Proactive study and novel mitigation of MV power system damage due to sub-power-frequency ferro-resonance for a gas plant," in *2017 Petroleum and Chemical Industry Technical Conference (PCIC)*, pp. 487-496, 2017, doi: 10.1109/PCICON.2017.8188771.

[2] Y. Wang, X. Liang, I. R. Pordanjani, R. Cui, A. Jafari, and C. Clark, "Ferroresonance causing sustained high voltage at a de-energized 138 kV bus: A case study," in *2019 IEEE/IAS 55th Industrial and Commercial Power Systems Technical Conference (I&CPS)*, pp. 1-9, 2019, doi: 10.1109/ICPS.2019.8733347.

[3] I. Kazhekin and M. Kharitonov, "Prevention of ferroresonant processes in microgrid operating in island mode," in *International conference Ecosystems without borders*, pp. 86-94, 2022, doi: 10.1007/978-3-031-24820-7_8.

[4] X. Ding, K. Yang, W. Wang, B. Liu, X. Wang, J. Zhang, and D. Li, "Ferro-resonance analysis of capacitor voltage transformer with fast saturation damper," *Energies*, vol. 15, no. 8, p. 2791, 2022, doi: 10.3390/en15082791.

[5] J. Izykowski, E. Rosolowski, P. Pierz, and M. M. Saha, "Design of ferroresonance suppression circuit for capacitive voltage transformer-analytical approach supported by simulation," in *2016 Power Systems Computation Conference (PSCC)*, pp. 1-7, 2016, doi: 10.1109/PSCC.2016.7541021.

[6] S. Poornima, "Subharmonic ferroresonance mitigation in capacitive voltage transformer using meminductor," *Electrical Engineering*, vol. 106,no. 4, pp. 4387-4396, 2024, doi: 10.1007/s00202-023-02229-z.

[7] R. P. Pineda, R. Rodrigues, and A. A. Tellez, "Analysis and simulation of ferroresonance in power transformers using Simulink," *IEEE Latin America Transactions*, vol. 16, no. 2, pp. 460-466, 2018, doi: 10.1109/TLA.2018.8327400.

[8] V. Torres-García, N. Solís-Ramos, N. González-Cabrera, E. Hernández-Mayoral, and D. Guillen, "Ferroresonance modeling and analysis in underground distribution feeders," *IEEE Open Access Journal of Power and Energy*, vol. 10, pp. 583-592, 2023, **doi:** 10.1109/OAJPE.2023.3312640.

[9] R. Tarko, W. Nowak, J. Gajdzica, and S. Czapp, "Analysis of ferroresonance mitigation effectiveness in auxiliary power systems of high-voltage substations," *Energies*, vol. 17, no. 10, p. 2423, 2024, doi: 10.3390/en17102423.

[10] A. Heidary, K. Rouzbehi, H. Radmanesh, and J. Pou, "Voltage transformer ferroresonance: an inhibitor device," *IEEE Transactions on Power Delivery*, vol. 35, pp. 2731-2733, 2020, doi: 10.1109/TPWRD.2020.3005321.

[11] S.-K. Kim, Y.-H. An, B.-T. Jang, J.-K. Choi, N.-H. Lee, J.-Y. Han, and Y.-J. Lee, "Study on EMTP simulation applying dual reactor for prevention of the ferro-resonance and VT burnout in substation system," *KEPCO Journal on Electric Power and Energy*, vol. 1,no. 1, pp. 1-8, 2015, doi: 10.18770/KEPCO.2015.01.01.001.

[12] H. Radmanesh, "Distribution network protection using smart dual functional series resonance-based fault current and ferroresonance overvoltage limiter," *IEEE Transactions on Smart Grid*, vol. 9, pp. 3070-3078, 2016, doi: 10.1109/TSG.2016.2626152.

[13] Y. Zan, W. Qian, D. Jiandong, and T. Wangjing, "Nonlinear dynamic analysis and ZnO-based suppression of ferroresonance overvoltage in distribution network," in *2015 5th International Conference on Electric Utility Deregulation and Restructuring and Power Technologies (DRPT)*, pp. 1321-1325, 2015, doi: 10.1109/DRPT.2015.7432434.

[14] S. Poornima, "Inception of Jump resonance in Single phase transformer," in *2021 4th Biennial International Conference on Nascent Technologies in Engineering (ICNTE)*, pp. 1-6, 2021, doi: 10.1109/ICNTE51185.2021.9487654.

[15] N. E. H. Fares, J. Sheef, T. Al-Malki, and T. Rajab, "Sub-cyclic damaging ferroresonant overvoltages in 230 kV transmission systems field experience of 230 kV transformer-ended cable feeders failure," in *2017 9th IEEE-GCC Conference and Exhibition (GCCCE)*, pp. 1-9, 2017, doi: 10.1109/IEEEGCC.2017.8448266.

[16] S. Seyedtabaii, "Mathematical modeling of passive techniques designed for PT ferroresonance suppression," *International Journal of Electrical Power and Energy Systems*, vol. 168, p. 110699, 2025, doi: 10.1016/j.ijepes.2025.110699.

[17] E. Cazacu and L. Petrescu, "Power quality issues generated by the nonlinear resonance occurrence in electric networks," in *2022 International Conference and Exposition on Electrical And Power Engineering (EPE)*, pp. 023-026, 2022, doi: 10.1109/epe56121.2022.9959753.

[18] Y. Wang, X. Liang, I. R. Pordanjani, R. Cui, A. Jafari, and C. Clark, "Investigation of ferroresonance causing sustained high voltage at a de-energized 138 kV bus: A case study," *IEEE Transactions on Industry Applications*, vol. 55, pp. 5675-5686, 2019, doi: 10.1109/TIA.2019.2936185.

[19] J. Correa and J. Vega, "Protection relay for secondary ferroresonance suppression in coupling capacitor voltage transformers," in *2020 IEEE PES Transmission and Distribution Conference and Exhibition-Latin America (T&D LA)*, pp. 1-6, 2020, doi: 10.1109/TDLA47668.2020.9326165.

[20] R. J. Hepziba, G. Balaji, R. Muralikrishna, and S. Rathinavel, "A case study on transformer ferroresonance for subsea cable connected 230 kV substations using PSCAD," *Electric Power Systems Research*, vol. 230, no. 1, p. 110192, 2024, doi: 10.1016/j.epsr.2024.110192.

[21] Z. Abdul-Malek, A. H. Khavari, M. Moradi, and C. L. Wooi, "Assessment of series compensator for ferroresonance damping in power system," *Applied Mechanics and Materials*, vol. 818, pp. 74-78, 2016, doi: 10.4028/WWW.SCIENTIFIC.NET/AMM.818.74.

[22] M. Sanaye-Pasand, H. Mohseni, S. Farhangi, A. Rezaei-Zare, and R. Iravani, "Effects of grading capacitors of CBs on inception ferroresonance in power transformers," in *39th International Universities Power Engineering Conference*, vol. 2, pp. 860-868, 2004, doi:10.1109/UPEC.2004.192470.

[23] R. Rüdenberg, "Transient performance of electric power systems: phenomena in lumped networks," *(No Title)*, 1950.

[24] Z. Ali, S. A. Peng, and M. Norfauzi, "Graphical analysis of ferroresonance modes in a voltage transformer energized through grading capacitance using correlation function," in *TENCON 2015-2015 IEEE Region 10 Conference*, pp. 1-5, 2015, **doi:** 10.1109/TENCON.2015.7373195.

[25] P. G. Khorasani and A. Deihimi, "A new modeling of Matlab transformer for accurate simulation of ferroresonance," in *International Conference on Power Engineering, Energy and Electrical Drives*, pp. 529-534, 2009, doi: 10.1109/POWERENG.2009.4915249.

[26] M. N. S. Mitra Patel, "Simulation and analysis of ferroresonance in power system," *International Journal of Innovative Research in Science, Engineering and Technology*, vol. 5, 2016, doi: 10.1109/IEMRE52042.2021.9386880.

[27] R. S. Pal and M. Roy, "Study and verification of ferroresonance simulated with Rudenburg's method," in *2021 Innovations in Energy Management and Renewable Resources (52042)*, pp. 1-5, 2021, doi: 10.1109/IEMRE52042.2021.9386880.

[28] S. Kim, B. Sung, S. Kim, Y. Choi, and H. Kim, "A study on ferroresonance mitigation techniques for power transformer," in *Proceedings of the International Conference on Power System Transients (IPST)*, pp. 1-7, 2015.
[29] G. B. Kumbhar, S. Alam, and N. Singh, "Effect of source voltage and core losses on ferro-resonance in transformer," *International Journal of Engineering Research*, vol. 3, 2014.
[30] B. Fan, G. Yao, W. Wang, X. Zeng, J. M. Guerrero, K. Yu, and C. Zhuo, "Principle and control design of a novel hybrid arc suppression device in distribution networks," *IEEE Transactions on Industrial Electronics*, vol. 69, pp. 41-51, 2021, doi: 10.1109/TIE.2021.3050390.
[31] A. M. Abdel-Hamed, M. M. El-Shafhy, and E. A. Badran, "High ohmic reactor as a shunt limiter (HOR-SL) method for ferroresonance elimination in the distribution system," *IEEE Access*, vol. 10, pp. 134217-134229, 2022, **doi:** 10.1109/ACCESS.2022.3231190.
[32] A. Bakhshi, M. Bigdeli, M. Moradlou, B. Behdani, and M. Hojabri, "Innovative solid-state ferroresonance-suppressing circuit for voltage transformer protection in wind generation systems," *Energies*, vol. 16, no. 16, p. 7684, 2023, doi: 10.3390/en16237684.

BIOGRAPHIES OF AUTHORS

Mohammed Boukaf is a Ph.D. student at the University of Mouloud Maamri, Tizi Ouzou, Algeria, specializing in electrical engineering. He was born in Algeria in 1987. He received the master degrees in electrical engineering from M'hamed bougara University, boumerdes, Algeria, in 2011. His research interests include electrical power systems. He can be contacted at email: mohammed.boukaf@ummto.dz.

Saliha Boutora received the B.Sc. degree in electrical networks from the University Mouloud Maameri of Tizi Ouzou, Algeria, the M.Sc. degree in high voltage engineering from Cairo University, Egypt, and the Ph.D. degree in electrical engineering from the Institute of Electrical and Electronic Engineering, University M'hamed Bougara, Algeria. She is currently an associate professor in the department of power and control, in the Institute of Electrical and Electronic Engineering, University M'hamed Bougara, Algeria. She is a member of the Laboratory of Signals and Systems, Boumerdes, Algeria. She can be contacted at email: s.boutora@univ-boumerdes.dz.

Hamid Bentarzi is a full professor at the University of M'hamed Bougara Boumerdes, specializing in electronic and electrical engineering. He earned his Electrical Engineering and Magister Degrees from INELEC, Boumerdes, and completed his Ph.D. in Microelectronic Systems at the ENP, Algiers. Since 2001, he has led a research team at the Signal and System Laboratory in Boumerdes, focusing on microelectronic systems applied to power systems and later became the laboratory director. His research interests include microelectronics, electrical protection systems, and smart grids, with significant contributions in developing technologies for monitoring and protecting smart grid elements. He has published over 200 technical papers, authored and edited four books, and actively participated in various national and international conferences. Hamid has supervised many researchers and Ph.D. students in these areas. He can be contacted at email: h.bentarzi@univ-boumerdes.dz.